Excited States in the ^{39}K and ^{39}Ca Mirror Pair

by Thomas Andersson

February 1999

Supervisors:
Prof. Claes Fahlander
Dr. Dirk Rudolph

Department of Physics
Division of Cosmic and Subatomic Physics
Lund University
Sölvegatan 14
223 62 Lund

Abstract

The mirror nuclei ^{39}K and ^{39}Ca were studied using data from a GAMMASPHERE experiment. The 4π charged-particle detector MICROBALL and several neutron detectors were included. The fusion-evaporation reaction ^{28}Si + ^{16}O is forming the compound nucleus ^{44}Ti which then decays populating high-spin states in the $A = 40$ mass region. The level schemes for the mirror nuclei were extended considerably. Tentative spins and parities were deduced by analyzing directional correlations of oriented states (DCO ratios) for ^{39}K.

Contents

1 Introduction

The ^{39}K and ^{39}Ca nuclei have, respectively, one proton and one neutron less than the $N = Z = 20$ doubly magic nucleus ^{40}Ca. Assuming that both protons and neutrons are nucleons with identical behaviour, and because of the charge-symmetry of the nuclear force, one expects the nuclei ^{39}K and ^{39}Ca to have a similar structure with equal energies and level spacings. The only difference arises from the electromagnetic interaction: Since ^{39}K has one proton less than ^{39}Ca, the Coulomb energies and, consequently, the excitation schemes of the nuclei differ slightly. By studying nuclei close to the nucleon numbers $N = Z = 20$, i.e., in the vicinity of ^{40}Ca, it is possible to deduce interesting properties for the nuclear shell model, e.g., neutron-proton interactions and single-particle energies. Furthermore, since the nuclei studied in this work lie only one hole away from ^{40}Ca, the properties of this nucleus can also be interpreted. Even though some nuclei around ^{40}Ca are stable, and quite easy to reach with nuclear reactions, the high-spin and high-energy states of most of these nuclei are still poorly investigated, but by using fusion-evaporation reactions these states can be reached.

The aim of the analysis was to extend the known level schemes for ^{39}K and ^{39}Ca and, for the latter weakly populated $N < Z$ nucleus, also to verify the assigned γ-ray transitions. The analysis was then followed by a comparison between the nuclei in order to, as mentioned above, verify specific parts of the shell model, including various basic assumptions on single particle excitations. Basically only two different data sets were needed: one for ^{39}K and one for ^{39}Ca. However, to be able to produce clean final spectra, and also in order to deduce the DCO ratios, data for other nuclei (which can be seen in Figure 1) were used in addition.

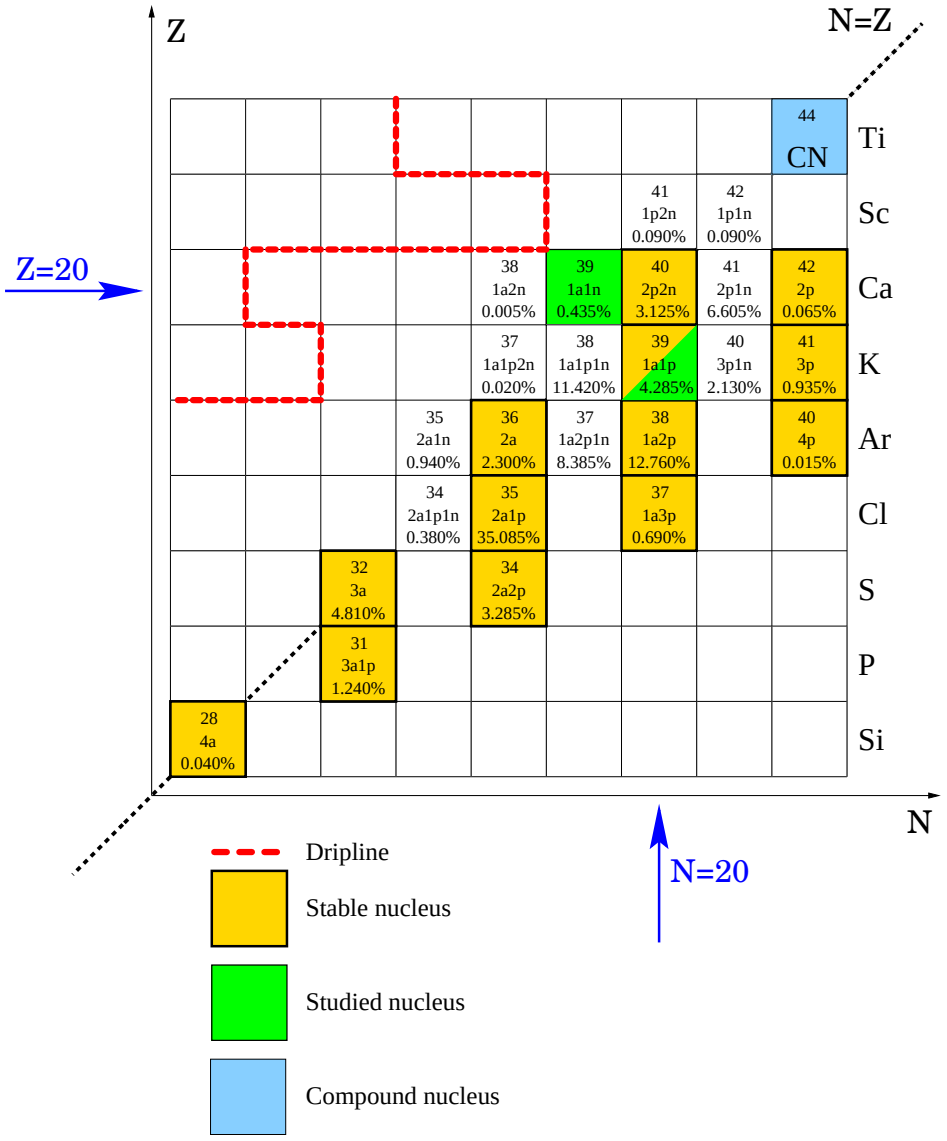

Figure 1: A part of the nuclidic chart providing the different reaction channels of the experiment, following the fusion-evaporation reaction ^{28}Si + ^{16}O at 125 MeV beam energy. The evaporated light particles are presented in conjunction with predicted (computer-simulated) relative cross-sections for each isotope. Stable isotopes are shown with thick border. The two shaded channels in the figure, 1α1p and 1α1n, correspond to the nuclei ^{39}K and ^{39}Ca, respectively, analyzed in this work. The top-most value in each square denotes the mass number A.

2 The Experiment at GAMMASPHERE

The data set that was used for the analysis in this work was obtained from a GAMMASPHERE experiment carried out in spring 1997 at the 88-inch Cyclotron at the Lawrence Berkeley National Laboratory. The original experiment used the reaction ^{28}Si + ^{40}Ca with a beam energy of 125 MeV (about 4.5 MeV per nucleon) to reach the compound nucleus ^{68}Se. However, the 0.5 mg/cm^2 thin self-supporting ^{40}Ca target (enriched to 99.9%) suffered from considerable oxidation. The large natural abundance of ^{16}O gave rise to an additional data set resulting from the reaction ^{28}Si + ^{16}O. In fact, the oxidation was so pronounced that nearly half of the data taken during the beam time came from this reaction. The two nuclei fused together to form the compound nucleus ^{44}Ti. The compound nucleus then rapidly decays ($\sim 10^{-20}$s) via emission of protons, neutrons and α-particles. For example, via emission of one α-particle and one proton (the 1α1p channel) ^{39}K nuclei are produced, or ^{39}Ca nuclei via the 1α1n channel (see Figure 1).

2.1 GAMMASPHERE and MICROBALL

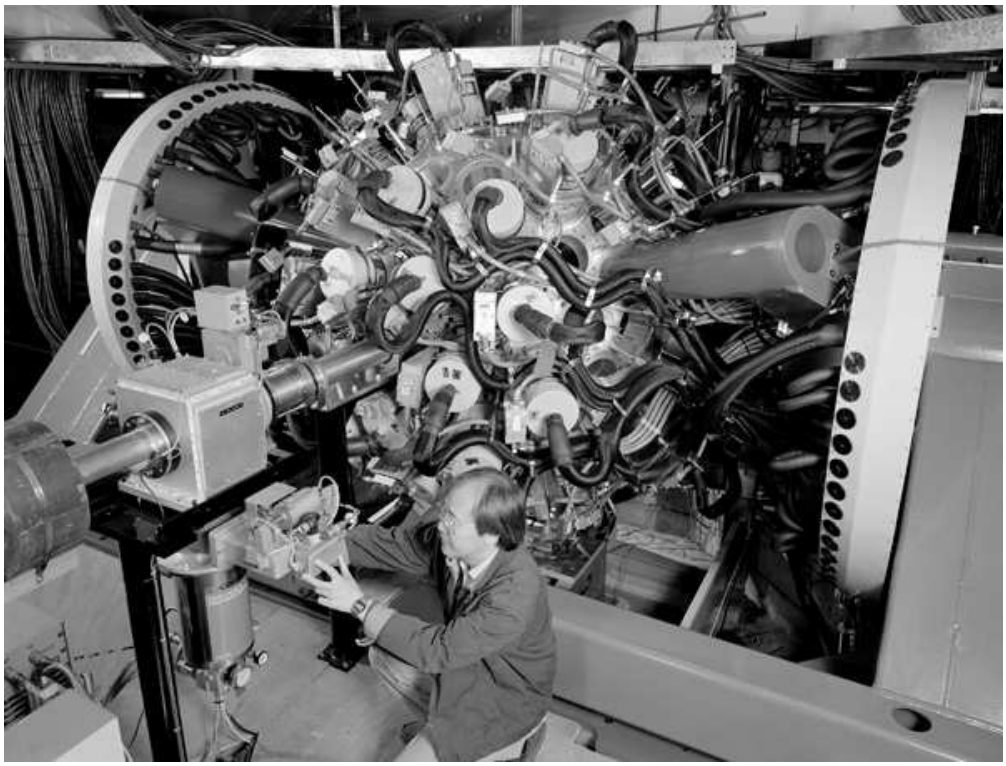

Figure 2: GAMMASPHERE. Figure from the GAMMASPHERE homepage.

As the name suggests, GAMMASPHERE was constructed to detect γ-rays, i.e., nuclear electromagnetic radiation. Its full implementation consists of no less than 110 high-purity germanium (HPGe) semiconductor detectors placed in a spherical shell. These HPGe crystals provide the best compromise of properties for a γ-ray detector, namely moderate detection efficiency combined with high energy resolution. Another important factor is the granularity, which provides the ability to localize individual γ rays and reduces the risk of detecting more than one hit in the same event in the same detector. Each of the HPGe detectors is also enclosed in a shield of bismuth germanate (BGO) scintillator crystals.

By rejecting events in which Compton-scattered γ-rays have deposited only part of their energy in the BGO detectors, a better peak-to-total ratio (P/T) can be achieved, so-called *Compton Suppression*. The advantage of using this technique is illustrated in Figure 3. The peak-to-total ratio (P/T) for a 1 MeV γ ray is increased from 0.25 without Compton suppression up to typically 0.60 when suppressed. Considering only single γ-rays, it may seem unnecessary to put so much effort into Compton suppression; the slight change in P/T (only about a factor of two) should not considerably improve the measurements. But since this kind of experiment often deals with high-fold coincidence measurements, the slightly improved P/T value becomes vital. For example, in a quadruple coincidence measurement, the P/T has to be raised to the fourth power, giving a total P/T improvement of approximately a factor 30.

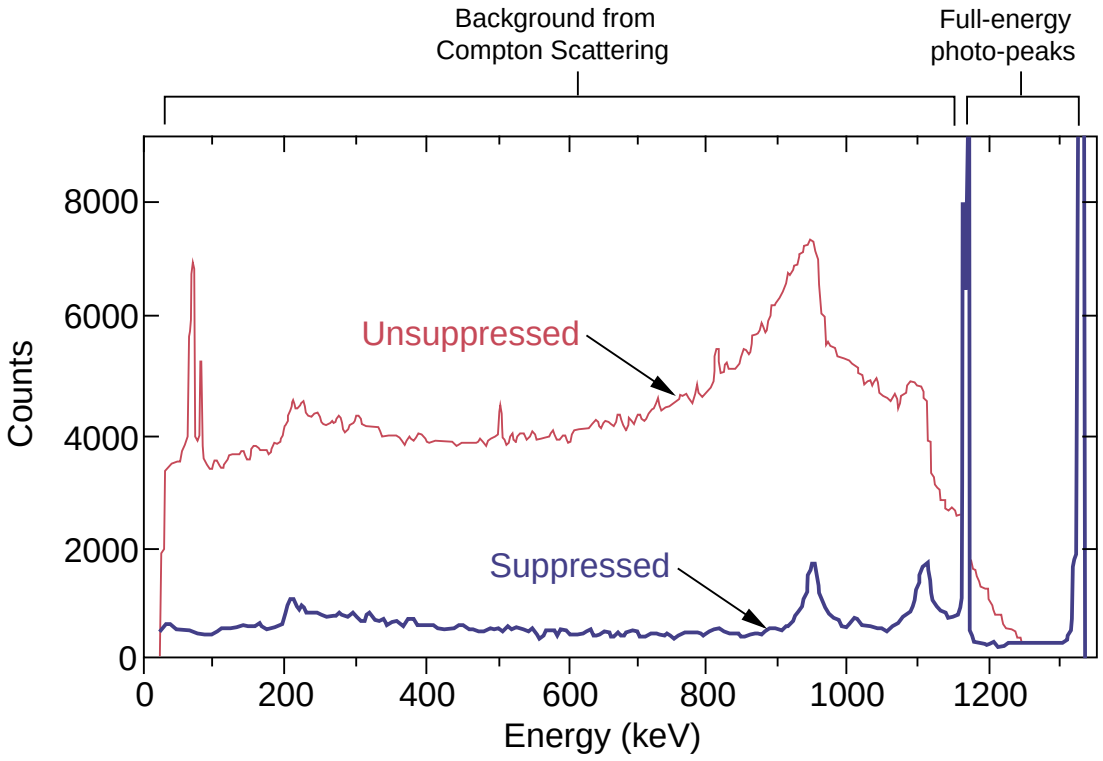

Figure 3: Illustration of the advantages using the Compton Suppression Technique. Figure taken from Ref. [1].

To further enhance the performance of GAMMASPHERE, several ancillary detectors can be added to the original HPGe configuration [1]. The experiment described in this work used GAMMASPHERE in conjunction with MICROBALL [2]. The MICROBALL, which is placed in the centre of GAMMASPHERE, consists of 95 CsI(Tl) scintillators placed in a near-spherical shell, covering 97% of the solid angle, see Figure 4. The purpose of adding this detector array was to be able to detect light-charged particles such as ^{1,2,3}H and ^{3,4}He emitted in the early stage of the fusion-evaporation reactions. The possibility to select different charged-particle decay channels has resulted in an enormous improvement of the sensitivity of Gammasphere, especially for experiments close to the $N = Z$ line. Reactions in this region often result in a high number of decay channels (see Figure 1) and thus, the possibility to distinguish between different channels considerably reduces the number of γ-rays, making detection of transitions belonging to a specific channel much easier. Also, MICROBALL has the capability of determining the directions of recoiling nuclei, and thus precise corrections for Doppler shifts can be made.

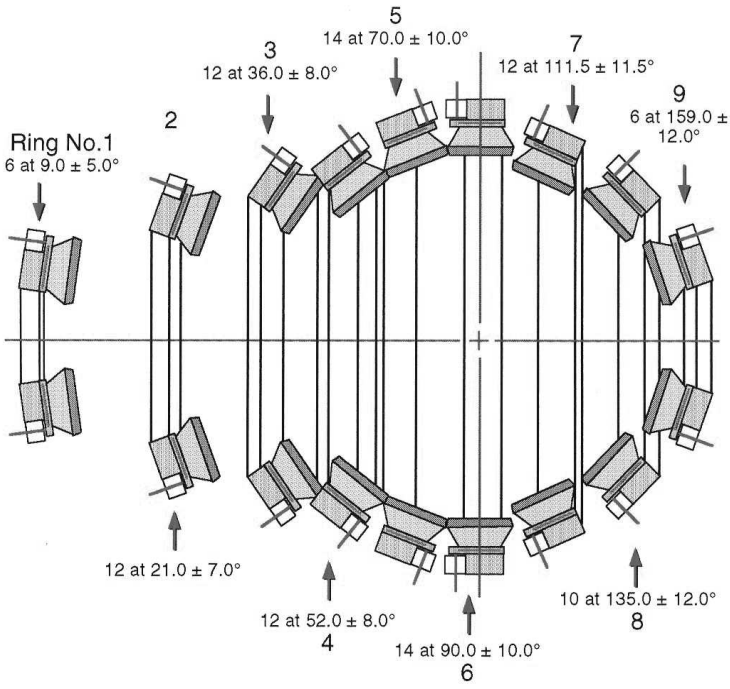

Figure 4: Schematic drawing of the 4π charged-particle detector system MICROBALL. The number of detectors and the angle coverage are shown. The beam goes from right to left, and the target is placed in the middle of ring no. 6. Figure taken from ref. [2].

In addition to MICROBALL, 15 liquid scintillator neutron detectors were used in the experiment. To make room for these neutron detectors, the three most forward HPGe detector rings had to be removed, leaving 83 γ-detectors. Table 1 shows how the germanium detectors were placed in the different rings for the experiment. Note that the angles of the rings have a reflection symmetry with respect to 90° relative to the beam axis. Although the use of neutron detectors implies an overall lower γ-ray detection efficiency, the additional channel selectivity is vital for studies of nuclei at or beyond the $N = Z$ line. If it were not for the neutron detectors, the ^{39}Ca nucleus would never have been identified and thus no analysis would have been possible. Further, by looking at the predicted cross-sections in Figure 1, the channels which are accompanied by neutron emission can be seen to have lower cross-sections. The

geometrical efficiency for detecting a neutron was about 5%, and as can be seen from the intensity axes in Figure 5, the effective efficiency is about 10%. Thus, by demanding a neutron the intensity typically drops a factor of ten. In these reactions, the recoil of the decaying neutrons, viewed in the laboratory system, is mainly concentrated to the forward direction. This explains why the effective efficiency can be greater than the geometrical: the distribution is anisotropic.

3 Analysis

Since a master thesis project is strongly limited in time, it is not possible to perform every single step in the data analysis of an experiment performed with such complex detector systems as GAMMASPHERE or EUROBALL. Thorough presorting and pre-selection of the data, including calibrations, energy gain matching, careful particle gating etc. of more than 100 detectors typically takes several months. Therefore, almost all data used in the analysis was already sorted beforehand, into matrices and spectra suitable for immediate $\gamma\gamma$ and $\gamma\gamma\gamma$ coincidence analysis.

3.1 The Identification of ^{39}Ca

One part of the analysis was to extend the known level scheme of ^{39}Ca [6]. The 1α0p1n gated projection spectrum in Figure 5 (middle) together with the known energy of the 2795 keV ($7/2^- \rightarrow 3/2^+$) ground state transition in ^{39}Ca from previous work were used as starting points. (Since doubly magic nuclei are known to be very strongly bound, an energy of approximately 3 MeV is needed in order to excite particles across the $N = Z = 20$ shell gap.) As can be seen from the intensities of the γ-ray intensities in Figure 5 the ^{39}Ca channel is very weak compared to other channels, as indicated by the predicted cross-sections in Figure 1.

The top part of Figure 5 shows the 1α0p γ-ray spectrum, i.e., without demanding a neutron. Actually, 1α0p means that any number of neutrons (zero, one or two) is allowed. The only requirement is that exactly one α-particle and exactly one proton was detected. This notation is hence only a practical convention that suits the purposes for naming spectra, and will be used through-out this work when discussing spectra.

As can be seen, the 1α0p spectrum is dominated by γ-rays from pure charged-particle channels, especially the 1α1p channel ^{39}K (347, 757, 887, 1130 and 2813 keV), but also the 1α2p channel ^{38}Ar (106, 670, 1642 and 2168 keV) and the 2α1p channel ^{35}Cl (971, 2244 and 3163 keV). Only reasonably strong neutron channels, like the 1α1p1n channel ^{38}K (1296 keV), can also be seen. The occurrence of all these channels in the 1α0p γ-ray spectrum is a result of the particle detection not being perfect. For example, in the case of ^{39}K one proton was not detected. Referring to the explanation of the notation above, what can be seen in Figure 5 (top) are channels reached by decay of one α-particle and possible additional particles. The middle part of Figure 5 shows the same kind of spectrum as above, but in addition demanding that one neutron be detected. Here the pure charged-particle channels have essentially disappeared. In addition to ^{39}Ca, only the strongest neutron channels, ^{38}K and ^{37}Ar, occur in the spectrum. However, now we observe the 2795 keV ground state transition of ^{39}Ca, which was not visible in the top spectrum. By demanding the detection of a neutron, the intensity typically decreases by about one or two orders of magnitude, but one gains considerably in sensitivity. Finally, the bottom part of Figure 5 shows a spectrum resulting from a coincidence gate set at 2795 keV in the 1α0p1n matrix.

Several peaks in the 2795 keV gated spectrum are clearly seen, and the statistics has dropped about another two orders of magnitude. On the other hand we have now selected only events in the 1α0p1n channel. The peaks seen in the bottom part of Figure 5 are strong candidates for transitions in ^{39}Ca. Assuming that the particle detection efficiency does not significantly depend on the particle

multiplicity, i.e., the reaction channel, the intensity for a γ-ray transition in different particle-gated spectra depends only on the detection efficiency and the number and kind of emitted particles. By taking the intensity ratio for a specific γ ray in two differently gated particle spectra, and comparing this ratio to reference ratios from known nuclei, the transitions belonging to a certain cascade can be assigned to a specific reaction channel. In this case we want to prove that the lines found by gating on the ground state transition of ^{39}Ca belong to the 1α0p1n channel.

To show that the transitions belong to a 1α channel (i.e., those nuclei produced via the decay of one α-particle), the intensities for the γ rays in the 1α0p1n and the 0α0p1n spectra were determined. The same procedure was performed for the reference nuclei. For example, the 1α2p and the 0α2p spectra were used to determine intensities for the transitions of the 1α channel ^{38}Ar. Then the same ratio $R_\alpha = I(1\alpha\gamma\gamma)/I(0\alpha\gamma\gamma)$ was calculated for all nuclei and plotted in Figure 6. This ratio should be the same for all 1α channels, since all other particles involved in determining the intensities cancel each other; the spectra differ only in the respect that a different number of α-particles are demanded. Thus, it does not matter for what kind of 1*alpha*-channel the ratio is calculated. The ratio for 2α channels should differ from the 1α channel ratio, as should the ratio for the 0α channels (the nuclei produced via proton and/or neutron decay only). The ratio for the 0α channels should be identical to zero, since these channels should not at all occur in a 1α gated spectrum.

For the ^{39}Ca nucleus, as for the ^{39}K reference, the intensities for the α ratio were derived from gating on a lower energy γ-ray transition rather than on the ground state transition. To determine the ratio R_α it is necessary to use γ-gated spectra, originating from 1α- and 0α-gated matrices. For the 1α (or 2α) reaction channels, such as ^{39}Ca and ^{39}K, the lack of the detection of the α-particle in the latter matrix (0α) leads to significantly broader peaks, especially at higher energies. This is due to the incapability of calculating the kinematic correction, since no momentum information for the α particle is available. Thus, when a gate is set at a broadened peak, intensity may be lost if the gating width is kept constant. Consequently, the ratio $I(1\alpha\gamma\gamma)/I(0\alpha\gamma\gamma)$ will take on a higher value. The solution is either to make the gate wider, which would imply collecting a larger number of contaminating peaks in the spectrum, or to set the gate at a peak of lower energy in the cascade. The broadening is also noticeable at lower energies, but not as pronounced as for higher energy peaks. In addition, there are fewer peaks at $E_\gamma \lesssim 500$keV in this mass regime, providing cleaner gating conditions (not so many contaminating peaks). Therefore, for ^{39}Ca, the 252 keV transition was used for gating and for ^{39}K the 347 keV transition. Figure 6 proves that the transitions of interest (cf. bottom of Figure 5) can be assigned to the 1α-0p-1n channel ^{39}Ca. An analogous procedure was followed for the proton and neutron channels.

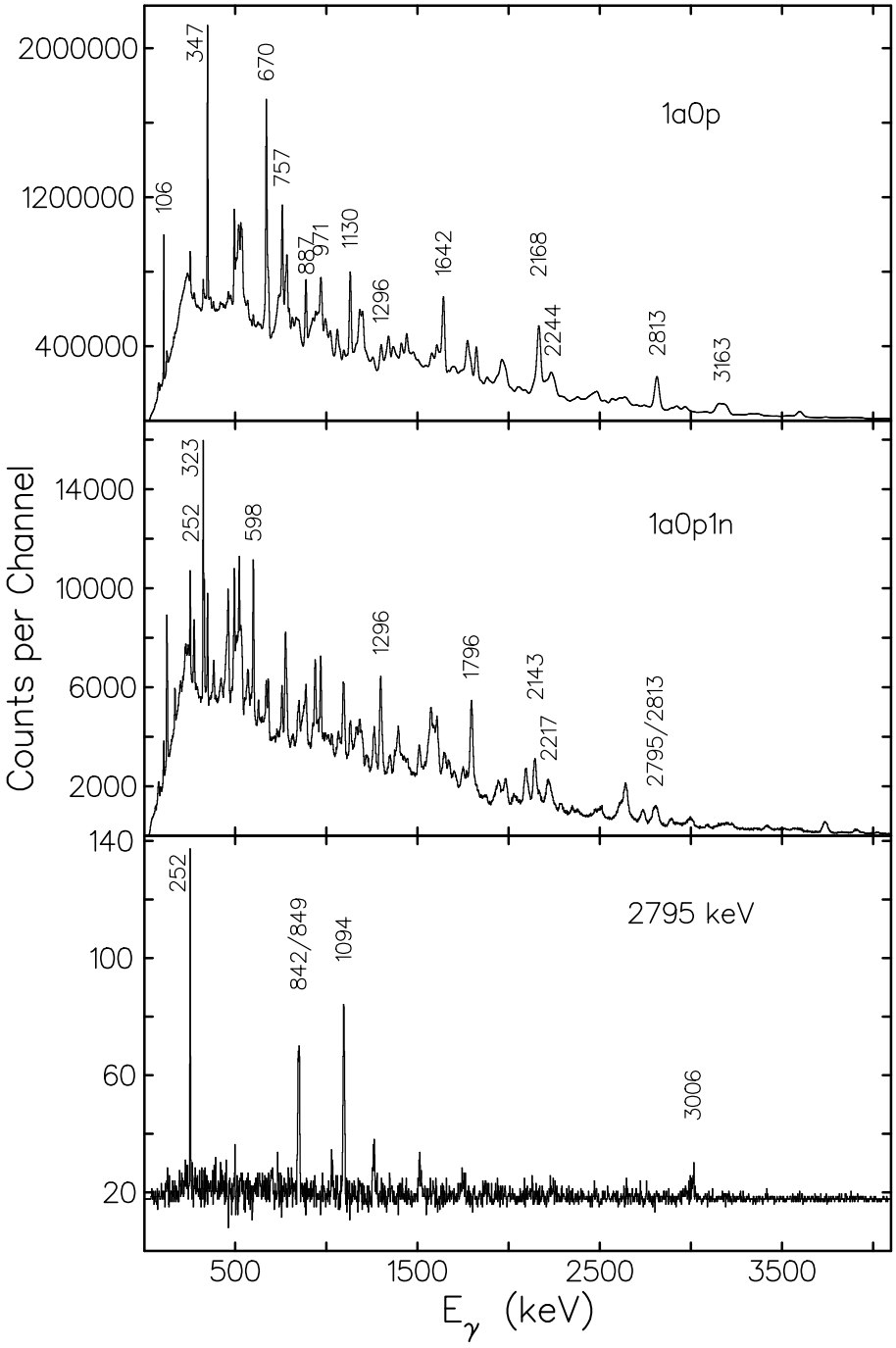

Figure 5: Top: γ-ray spectrum, demanding one α-particle and zero protons to be detected in MICROBALL. Peaks from ^{38}K, ^{39}K, ^{38}Ar and ^{35}Cl are dominating. Middle: γ-ray spectrum demanding also one neutron. Peaks from ^{39}Ca, ^{37}Ar, and ^{38}K. Bottom: 2795 keV gate in the 1α0p1n matrix. Peaks belonging to ^{39}Ca are totally dominating.

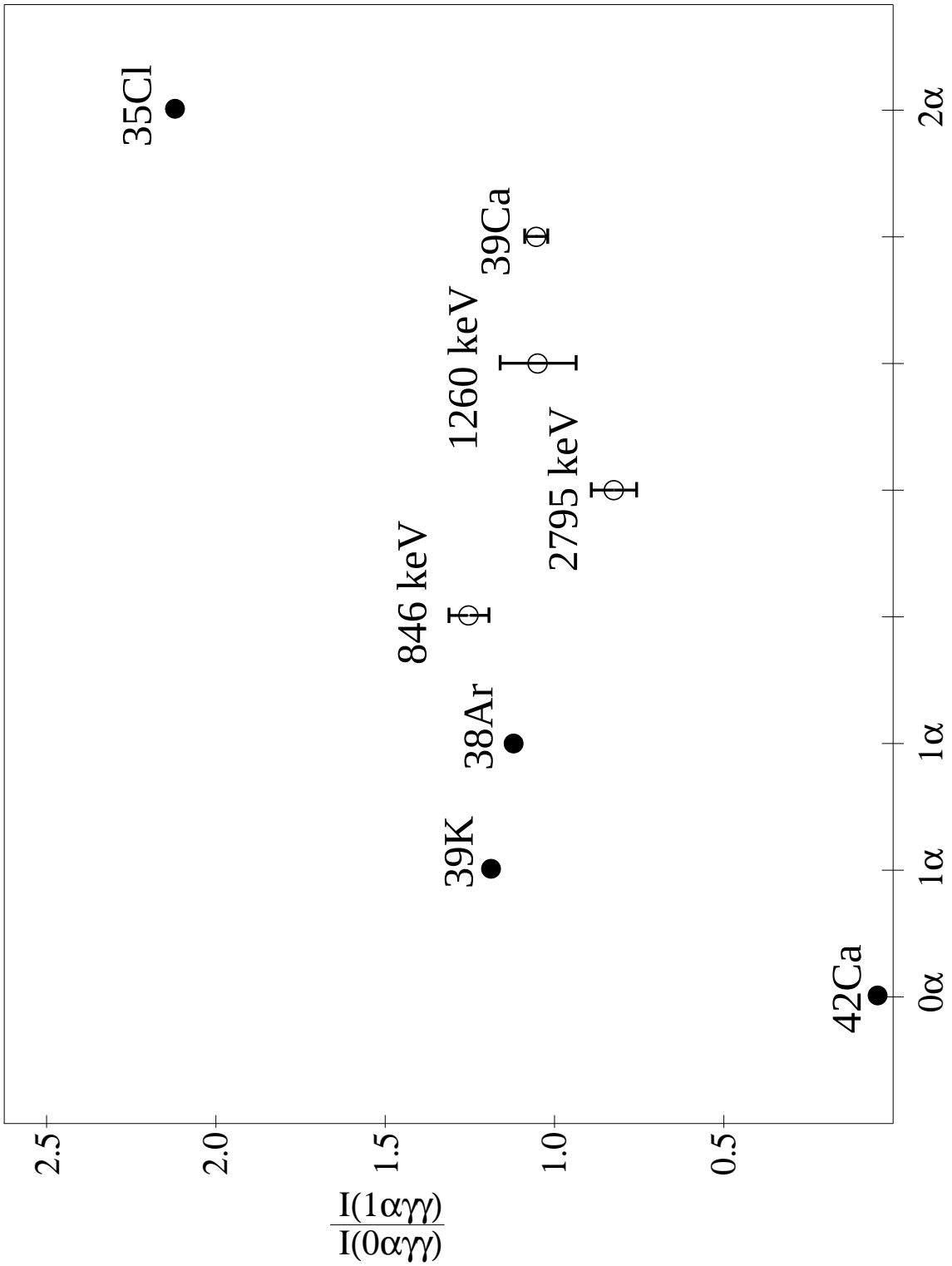

Figure 6: See caption on page 13.

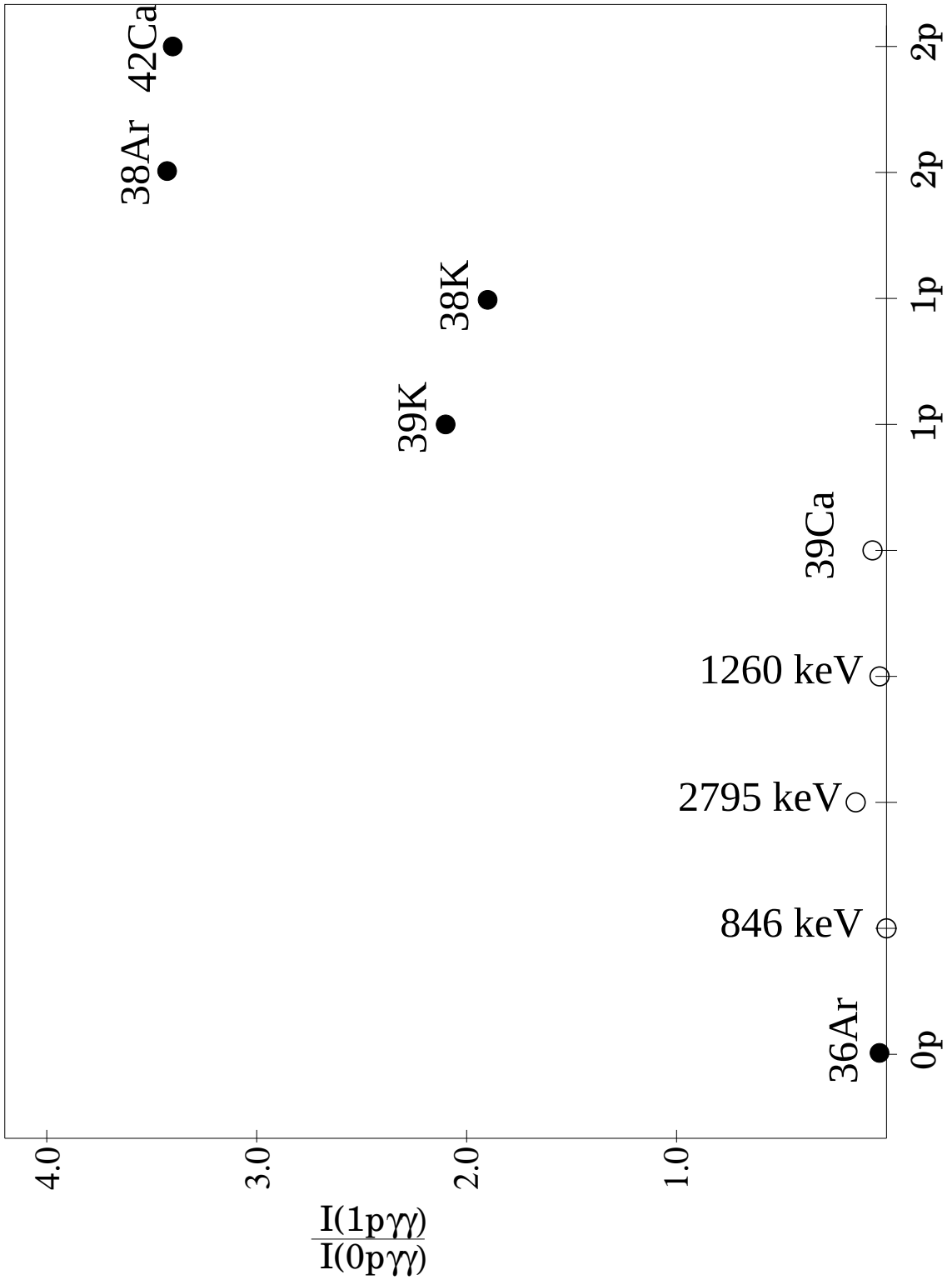

Figure 6: See caption on page 13.

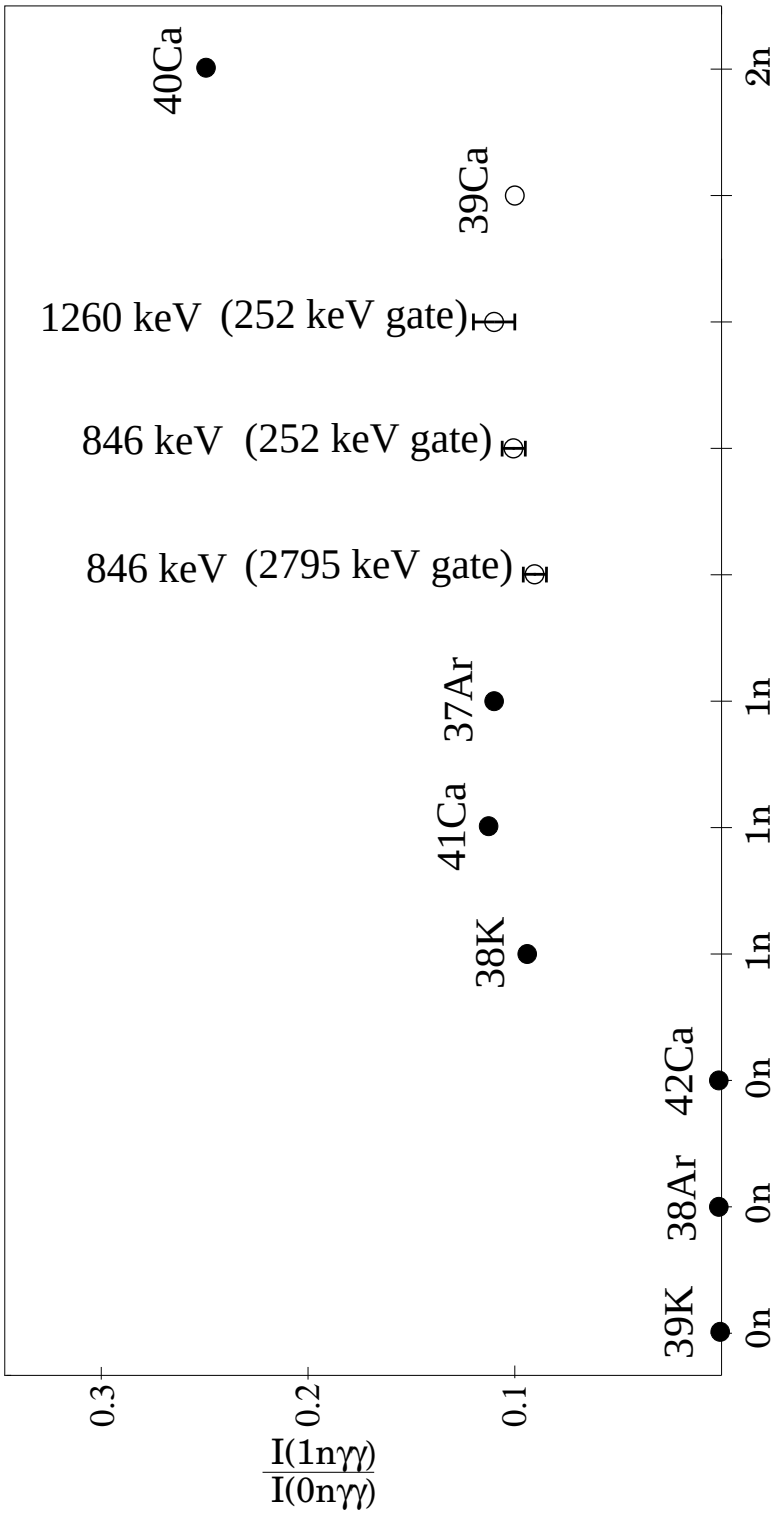

Figure 6: Intensity ratios for different α-particle, proton, and neutron multiplicities. References are plotted with filled dots, transitions belonging to ^{39}Ca are unfilled. The point marked ^{39}Ca is the calculated mean from the plotted ^{39}Ca transitions. The uncertainties for the proton multiplicities are smaller than the symbols. The '846 keV' point is calculated from the sum of the 842 keV and the 849 keV transitions.

3.2 The Level Scheme of ^{39}Ca

After having assigned the transitions in Figure 5 to ^{39}Ca, they were to be placed in a level scheme. By using the RadWare program package [3], it is possible to use coincident data from $\gamma\gamma$-matrices or $\gamma\gamma\gamma$-cubes to deduce a level scheme. A $\gamma\gamma$-matrix contains all events with at least two γ-rays E_{γ_1} and E_{γ_2} detected in GAMMASPHERE in coincidence with the selected evaporated particles. For every such selection of particles a $\gamma\gamma$-matrix can be made. Correspondingly, a matrix in three dimensions is called a cube. The LEVIT8R cube analysis program also provides both γ-ray energies and consistency checks of their intensities. After having confirmed the strongest 2795 keV transition as the ground state transition, single and double γ-gating both in the LEVIT8R cubes and by hand in a 1α0p1n $\gamma\gamma$-matrix helped putting the other transitions that were found into the level scheme, illustrated in Figure 7. First, a gate was set in the 1α0p1n matrix on the 2795 keV ground state transition. This spectrum was then cleaned from the weak but present ^{39}K contamination by subtracting a fraction of the 2813 keV ground state transition gated 1α0p1n spectrum. The spectrum was further cleaned by subtracting the 2795 keV gated spectrum originating from the 1α1p1n matrix, resulting in the spectrum shown in Figure 5 (bottom). The transitions found in this clean ^{39}Ca reference spectrum or gated on in the following and cleaned in a similar manner were put into a table showing $\gamma\gamma$ coincidences (Table 2), to easier see which transitions were in coincidence. Fits to the peaks in the summed spectrum from the 252, 842, 1094, and 2795 keV gated spectra and in the 1α0p1n gated spectrum were performed in order to determine the relative intensities. The final result is shown in Figure 7 and data for all transitions is summarized in Table 3. A total of 7 new transitions were placed in the level scheme.

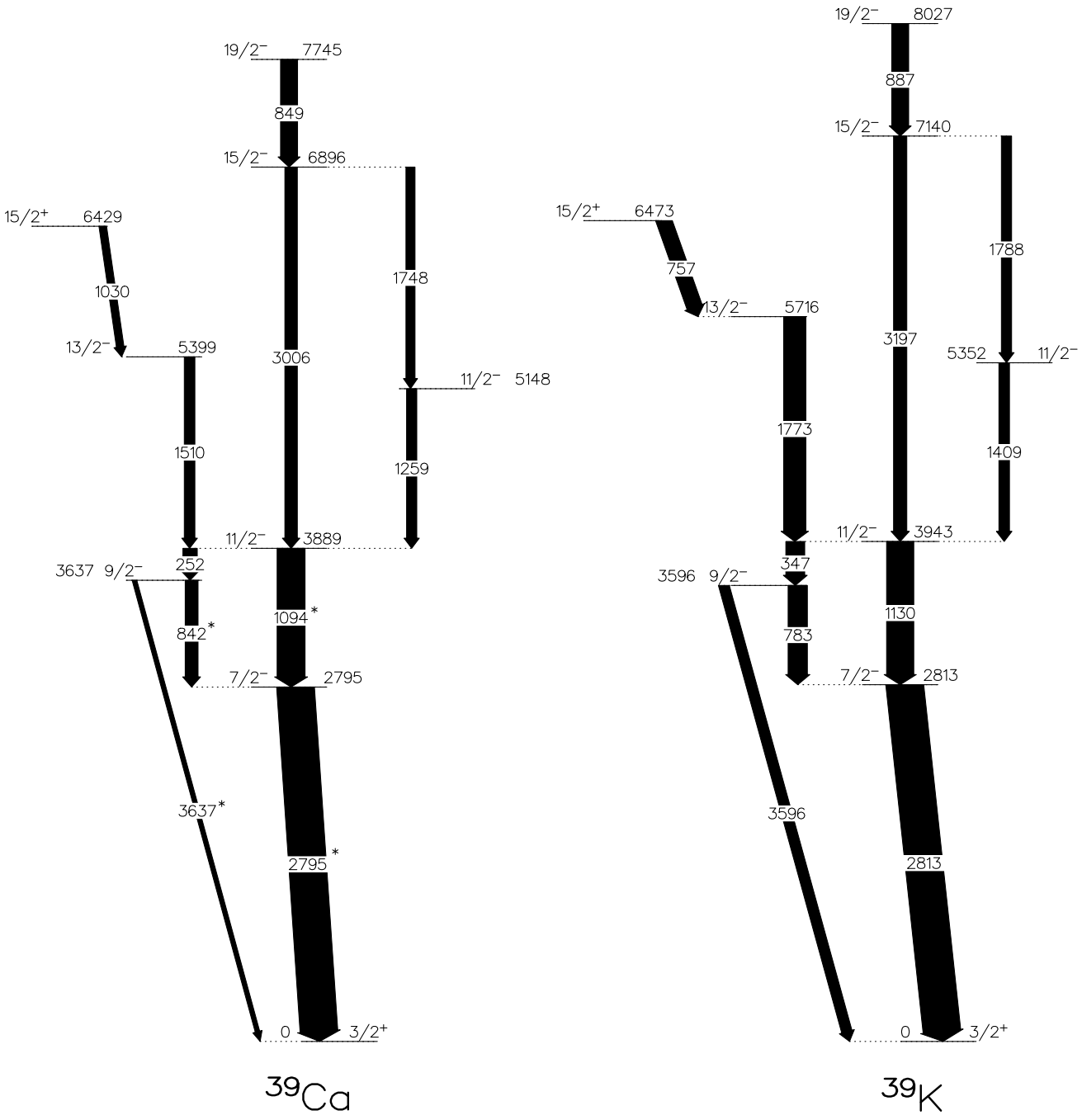

Figure 7: The proposed level scheme for ^{39}Ca, compared to the mirror states in ^{39}K. Previously known transitions in ^{39}Ca are marked with an asterisk. All shown transitions in ^{39}K were previously known. Spin and parity assignments for the new levels in ^{39}Ca are based on the mirror symmetry.

3.3 DCO ratios

The assignment of multipolarities to the different γ transitions, and hence spins to the corresponding states, require the use of angular distribution and/or angular correlation techniques. In the experiment the multipolarities were extracted by grouping the germanium detectors into so-called 'pseudo'-rings, mainly in order to increase statistics. Four of these 'pseudo'-rings were created (see Table 1) : Ring "30" consists of the Ge detectors from the rings at 142.6°, 148.3°, and 162.7°, ring "53" of 50.1°, 58.3°, 121.7°, and 129.9°, ring "70" of 69.8° and 110.2°, and ring "83" of the Ge detectors at 79.2°, 80.7°, 90.0°, 99.3°, and 100.8°. In this work, only data from the "30" and "83" rings were used to deduce the multipolarities.

In fusion-evaporation reactions, like the one employed in this work, the residual nuclei have their initial spins aligned in a plane orthogonal to the beam axis. Therefore, the γ rays have an anisotropic angular distribution of their yields. Anisotropic emission is used for determining the angular *Directional Correlations of Oriented States*, the so-called DCO ratios [4, 5], for subsequent γ-rays in a cascade. Here they are defined as

$$R_{DCO}(30-83;\gamma_1\gamma_2) = \frac{I(\gamma_1 \textit{ at } 30°;\ \textit{gated with } \gamma_2 \textit{ at } 83°)}{I(\gamma_1 \textit{ at } 83°;\ \textit{gated with } \gamma_2 \textit{ at } 30°).} \quad (1)$$

In the GAMMASPHERE detector array a total of 83 Ge detectors were present. Thus, the maximum number of combinations of detectors for $\gamma\gamma$-detection can be estimated by $\binom{83}{2} \sim 3400$. To analyze DCO ratios, only the 15 detectors from ring "30" and the 23 detectors from ring "83" could be used, so the number of detector combinations is 345 (only some 10% of the maximum number used to construct the level scheme). Of course, since the detectors have been split into four pseudo-rings, it is in principle possible to investigate all combinations of these, and not only the 30°-83° combination. In this work, only the DCO ratios from the ring-combination as defined in Equation 1, which provides the most pronounced anisotropy effect, could be analyzed. Also, the calculations were only carried out for ^{39}K since the data for ^{39}Ca is lacking statistical accuracy. Events in the "30"-ring were sorted on the x-axis and events in the "83"-ring on the y-axis of a $\gamma\gamma$ matrix. Projections were made for both x and y. By gating on a specific transition in both directions of the $\gamma\gamma$ correlation matrix, and then fitting both the transitions present in the gated spectra, the DCO ratio could be calculated from the intensities. Corrections were also made for the slightly different relative detection efficiencies of the pseudo-rings. The DCO ratios are included in Table 4. Multipole assignments for the transitions are also shown in this table but should rather be interpreted as probable than as proved multipole assignments (except for the previously known transitions). However, it is still possible to make definite multipole assignments as is shown in a more in-depth discussion in Section 3.5. The multipole assignments have been derived by studying the DCO ratios and by considerations made to transitions in parallel.

The best kind of transition to make the gate on is a stretched (electric) quadrupole transition, E2. Then $R_{DCO} = 1.0$ can be expected for coincident stretched quadrupole transitions. A pure stretched $\Delta I = 1$ transition should have $R_{DCO} \sim 0.5 - 0.6$. However, E2 admixture to a M1 transition can cause DCO ratios between ~ 0.2 and ~ 2.0. DCO ratios in excess of ~ 1.3 can thus be used to safely assign stretched $\Delta I = 1$ transitions. A $\Delta I = 0$ transition typically gives $R_{DCO} \lessapprox 1.0$. Especially when the calculated values are not exactly within the ranges stated above, the multipolarity assignments are also based on yrast[1] arguments: The larger the intensity that feeds a state, the higher is its spin value with respect to excitation energy. For example, the 1773 keV transition is most probably a mixed (E2/M1)

[1] An interesting story about the 'physical' ethymology of this *Swedish* word can be found in *J. Robb Grover, Phys. Rev. Vol. 157, No. 4, May 20 1967*

$\Delta I = 1$ transition, since the value (see Table 4) is higher than 0.5 but significantly less than 1.0. (The amplitude of this mixing is given by the mixing ratio δ(E2/M1).) The yrast argument excludes $\Delta I = 0$. DCO ratios of different combinations of rings should a) vary for $\Delta I = 0$ transitions, and b) allow for the measurement of the mixing ratio δ(E2/M1). More about spin assignments in Sections 4 and 3.5.

3.4 The Level Scheme of ^{39}K

Much more was previously known for ^{39}K than for ^{39}Ca [6, 7]. This, of course, made it easier to get started with constructing the level scheme. A few low-spin transitions, for example the 2523 keV transition from the $1/2^+$ state to the $3/2^+$ ground state, could not be found in this data set because of the yrast arguments mentioned in Section 3.3; fusion-evaporation reactions populate preferably high-spin states along the yrast line. However, approximately 50 new transitions were found and added to the level scheme shown in Figure 10. One major problem was to suppress transitions from contaminating nuclei in the spectra; in the 1α1p projection spectrum (Figure 8 top) one can easily see transitions belonging to other nuclei, in this case mainly from the 1α2p channel ^{38}Ar, the strongest channel in this reaction (see Figure 1) and from the 2α1p channel ^{35}Cl. The gate on the 2813 keV ground state transition in the 1α1p matrix (Figure 8 bottom), however, provided a reference spectrum for ^{39}K. In principle, all peaks in that spectrum (but also only these) belong to ^{39}K; one can see that transitions from the other residual nuclei have disappeared.

To illustrate the construction of the level scheme, three transitions from different places in the level scheme will be discussed. The selection of spectra is mainly based on the desire to show regions of special interest, but also on the wish to illustrate clean gates; if every gate made were perfect, the selection of spectra would perhaps have been done slightly differently. Lack of intensity has played the most significant role in discarding some interesting transitions in the level scheme. All three gates below have been set in the 1α1p matrix. The resulting spectra are all illustrated in Figure 9 and the discussion below will refer to this figure and to the level scheme in Figure 10.

The first example is the 3197 keV transition from the $15/2^-$ level at 7140 keV to the $11/2^-$ level at 3943 keV. Since this transition is in strong coincidence with all transitions below 3943 keV, but not with the 1773 keV line, it must somehow be feeding the 3943 keV level. Assuming that the placement of the coincident 1788 keV and 1410 keV transitions from the 7140 keV level to the 3943 keV level is already known, a simple addition of their energies gives a value that fits the 3197 keV transition, within the uncertainties of the γ-ray energies. Thus, the 3197 keV transition should be placed in parallel to these two transitions, and this is also confirmed by looking at the spectrum; no coincidence is seen with either the 1788 keV or the 1410 keV transition. Further verification is provided by the obvious coincidences with the 887, 1881 and 2970 keV transitions, which are placed just above the 1788 keV transition. When putting the 3197 keV transition into the level scheme, the placement of the transitions above it was not known, but now it acts as a confirmation.

The next example is the 4066 keV transition feeding the same 3943 keV level as the 3197 keV transition discussed above. The lack of coincidences with the transitions feeding the 3943 keV level (1410, 1773, 2062, 2490, 3197 keV) implies that it constitutes a branch of its own. The only other coincident transitions are the ones situated above the 4066 keV transition, i.e., the 2256 and 2746 keV transitions. The fact that the 2004 keV and the 2655 keV transitions also were observed fixes the placement of the 4066 keV transition; the sum of 2062 keV and 2004 keV matches the energy of the 4066 keV transition.

As the last example the proposed 5105 keV high-energy transition is chosen. It illustrates the difficulty of placing transitions high up in the level scheme. The spectrum does not show many coincident transitions. However, the apparent increase in intensity for the 3597/3599 keV doublet peak

compared to the other gates tells us that the 5105 keV transition most probably is either fed or is feeding the 3599 keV transition at 13506 keV. The presence of the 1881 keV coincident transition, however, excludes the first case. If the first suggestion were true, we should also see the 2302 keV transition feeding the 9908 keV level in coincidence, which is not the case.

These examples illustrate some of the complexity in placing transitions. It is mostly not satisfactory with only one gate to place a transition; often many checks have to be done in many different gates to exclude or confirm coincidences, especially when the intensities drop. In order to find (and place) the transitions at high energy (with low intensity), the gates on the transitions below 3943 keV were added to increase statistics and thus make it easier to find new peaks.

3.5 Spin Assignments

As discussed in Section 3.3, assigning multipole orders for the transitions by only studying DCO ratios from one angle combination are not straight-forward, especially when the DCO ratios lie in the range between different multipole orders. A quick look at Table 4 reveals that the ratios calculated from different gates are not always consistent, if any at all could be extracted. This inconsistency or lack of calculated values is mainly a consequence of low statistics and/or of imperfect fits or gating. Also, by using only the DCO ratios, no information about the parity of the transitions can be extracted. However, studying the level scheme for ^{39}K in Figure 10 on page 22 offers a great deal of help for assigning multipole orders. By using the known multipole orders from the known transitions and the calculated DCO ratios, we can 'walk around' in the level scheme to try to solve some puzzles. If for instance one transition with known multipole order sits in parallel with two consecutive transitions we know that these latter two must have the same total spin difference as the known transition. So if the DCO ratios suggest two different multipole assignments for a transition, knowing the spin of a parallel transition can help us make the decision. In this section we will try to explain some of the arguments for assigning the multipoles shown in Table 4. The discussion below will refer to this table and to the level scheme in Figure 10.

First we will check that the DCO ratios confirm the known multipole assignments. The 2813 keV ground state transition has DCO ratios very close to 1.0 and can thus safely be assigned as a quadrupole. No conclusion can be drawn for the parity but since it was determined for both the ground state and for the 2813 keV level we know that this is an M2 transition [6, 7]. For the transitions just above the 2813 keV level the assignment is easier: the values for the 1130 keV transition are close to 1.0 and would thus be a $\Delta I = 2$ transition. This is confirmed since the DCO ratios are close to 0.6 for the parallel 347 keV transition (implying a $\Delta I = 1$ transition) and that the values for the 783 keV transition are far enough away from 1.0 to exclude a $\Delta I = 2$ or $\Delta I = 0$ transition; the total spin difference for this branch is hence also $\Delta I = 2$. Now the 3597 keV transition can also be assigned as an octupole.

In the case of the 1410 keV transition depopulating the 5352 keV level, the ratios from the 1130 keV and the 887 keV gates are consistent with each other and lie just below 1.0, implying a $\Delta I = 0$ transition. Here we disregard the ratio calculated for the 2813 keV transition, because of its non-negligable deviation from the other values. The 1788 keV transition on top of the 1410 keV transition have DCO ratios just above 1.0 and could have either $\Delta I = 1$ or $\Delta I = 2$ and the same is true for the parallel 3197 keV transition. Which of these is true we cannot yet say. We have to look for further ways to reach the 7140 keV level. The 2062 keV transition feeding the 3943 keV level has relatively low intensity, implying that the values were determined with too low statistical accuracy. Also, for the 1135 keV transition situated on top of the 2062 KeV transition no ratios could be calculated, because of low intensity. Thus we can draw no conclusions from these values. The two consecutive transitions with 1427 keV and 1773 keV may help us decide. The latter can quite safely be assigned as a $\Delta I = 1$ transition. Only one ratio is calculated for the 1427 keV transition but since it has a big uncertainty

it could well be a $\Delta I = 1$ transition. Thus we select the $\Delta I = 2$ possibility for the 1788 keV and the 3197 keV transitions. The remaining assignments were made by using the same procedure as above, however the assignments are more or less certain.

As can be seen in the level scheme many of the spin assignments are made tentatively. This is mainly a consequence of having too few calculated DCO ratios and too low statistical accuracy. If the calculations were carried out for more pseudo-rings (see Section 3.3) we would probably have a greater consistency for the DCO ratios. All the non-tentative spin assignments for the levels in Table 4 and Figure 10 were previously known, except for the $19/2^-$ level at 8027 keV, the $15/2^+$ level at 7567 keV and the $19/2^+$ level at 10303 keV, which have been assigned from the DCO ratios calculated in this work.

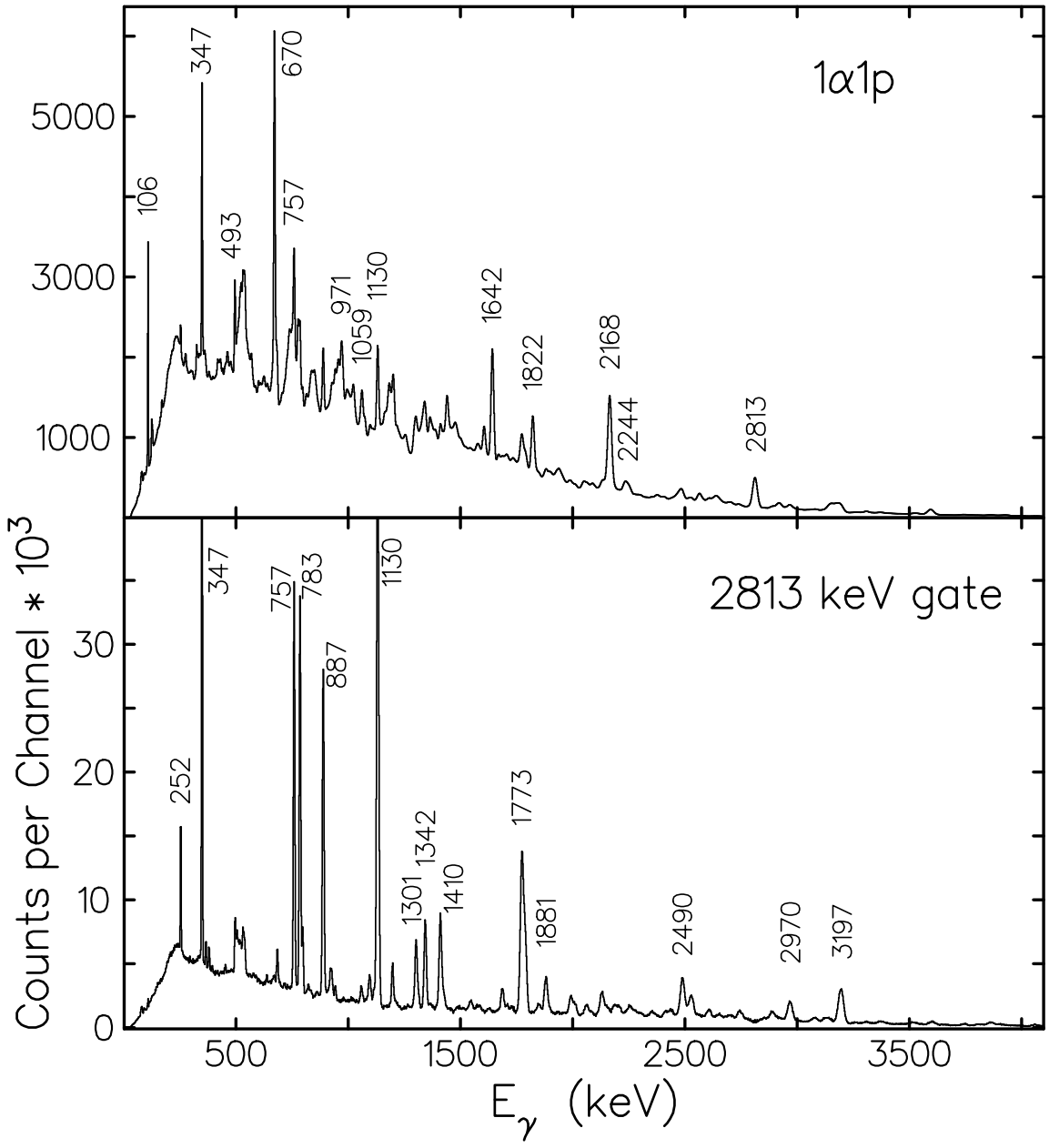

Figure 8: Top: γ-ray spectrum, demanding one α-particle and one proton to be detected. Peaks from ^{39}K (347, 757, 1130, 2813 keV) but also from the strong contaminating nuclei ^{38}Ar (106, 493, 670, 1642, 1822, 2168 keV) and ^{35}Cl (971, 1059, 2244 keV) are seen. Bottom: Cleaned 2813 keV gate in the 1α1p matrix illustrating coincident transitions in ^{39}K. Peaks belonging to contaminating nuclei have disappeared.

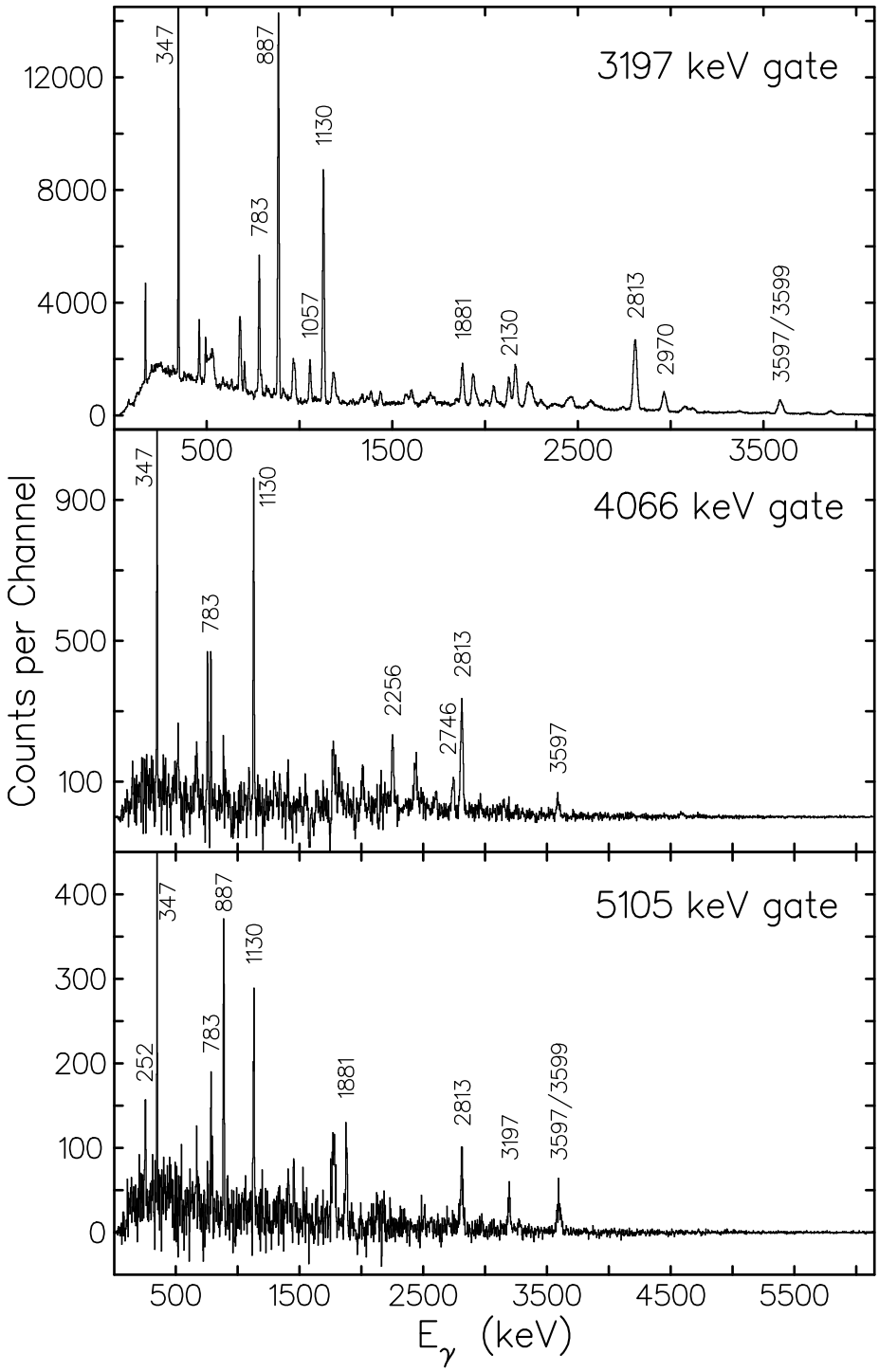

Figure 9: Gates set on the 3197, 4066 and 5105 keV transitions in the 1α1p matrix. The peaks for the strongest coincident transitions are marked. The peak marked 3597/3599 is a doublet. The relative intensities of these transitions can be determined by studying the number of counts, for example the top transition is some 40 times stronger in intensity than the bottom one. Please note the different energy scales.

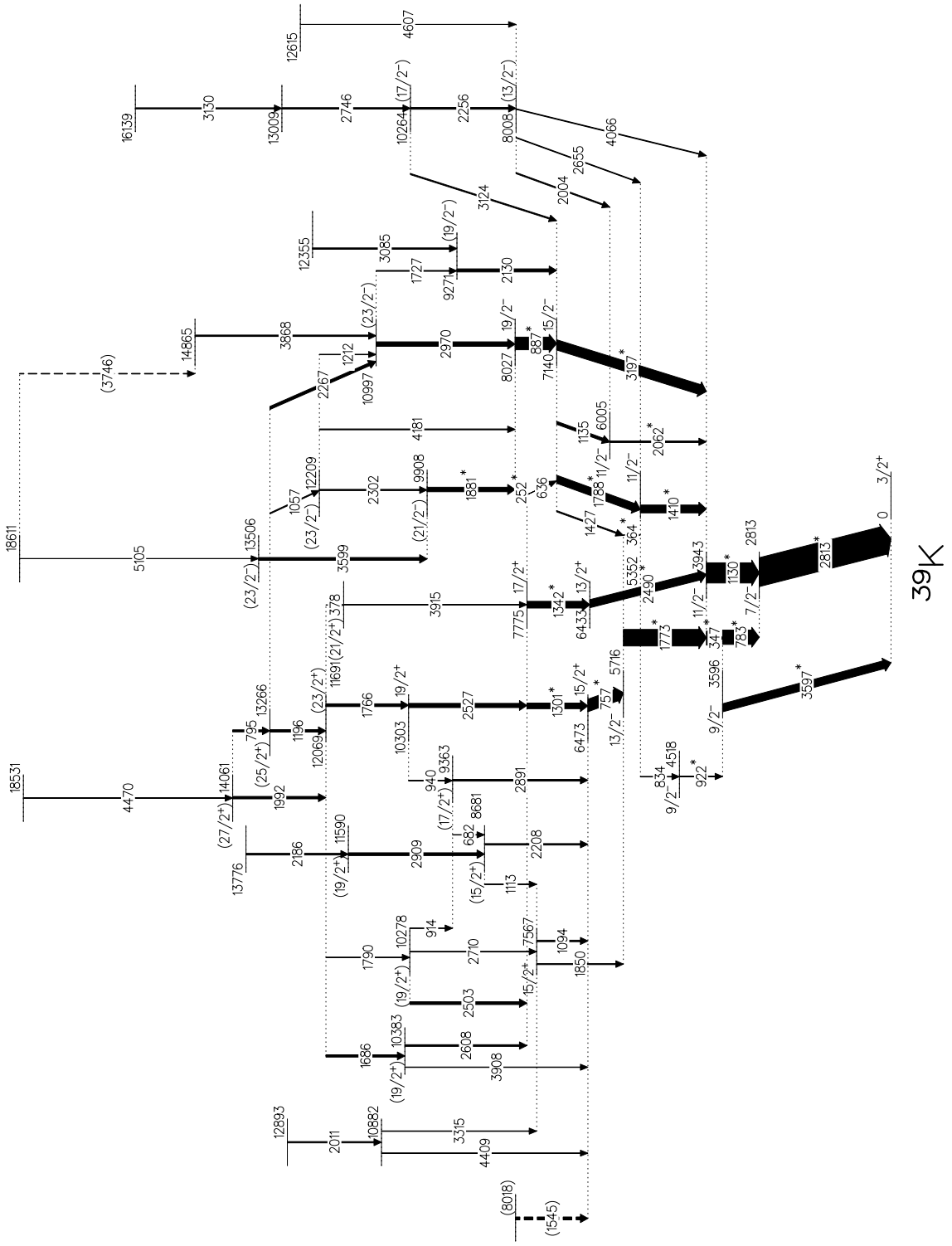

Figure 10: The proposed level scheme of ^{39}K. Previously known transitions are marked with an asterisk. The widths of the arrows correspond to the relative intensities of the transitions. Tentative transitions drawn with dashed arrows.

4 Discussion

4.1 Basic Excitations Across the $N = Z = 20$ Shell Gap

By calculating DCO ratios (see Section 3.3), spin assignments were confirmed or proposed for a number of levels in ^{39}K. Now we will try to understand why the levels should have these particular angular momenta. By exploring the different configuration possibilities that arise from the spherical shell model, one can quite easily understand most of the low-lying states in a spherical nucleus. A fundamental assumption of the shell model is that the motion of a single nucleon is due to the potential caused by all the other nucleons. In this way the other nucleons are allowed to occupy energy levels in a series of subshells. In the shell model one often also talks about magic numbers (2, 8, 20, 50, 82, 126), i.e., certain proton or neutron numbers with special properties. These numbers represent the closing of major shells. When a nucleus has either a major proton or neutron shell filled, it is considered to be more stable, since the energy gap to the next shell is large. A shell is defined as several energy levels lying close together with energy gaps above and below, clearly separating these levels from other states. One common potential used in the shell model is the Woods-Saxon potential

$$V_{central}(r) = \frac{-V_0}{1 + e^{(r-R)/a}}, \tag{2}$$

where R and a give, respectively, the mean radius and skin thickness of the nucleus. They are usually chosen to be $R = 1.25 \cdot A^{1/3}$ fm and $a = 0.524$ fm. This potential reproduces all magic numbers if a spin-orbit term is added to the total potential,

$$V(r) = V_{central}(r) + V_{\ell s}(r)\frac{\langle \ell s \rangle}{\hbar^2}, \tag{3}$$

and this term splits the degeneracy of the $n\ell$ shells. The spectroscopic nomenclature for a level is $n\ell$, where ℓ is the quantum number for the orbital angular momentum and n the radial quantum number. ℓ can take on the values $\ell = s, p, d, f, g, h, \ldots$ corresponding to $\ell = 0, 1, 2, 3, 4, 5, \ldots$ States with ℓ even have even parity and vice versa.

This ℓs coupling leads to the splitting of each $n\ell$ state and hence the states are denoted as $n\ell_j$ with $j = \ell \pm s = \ell \pm 1/2$ except for $\ell = 0$, in which case only $j = 1/2$ is allowed. Each $n\ell_j$ level is $(2j + 1)$ times degenerate. A more extensive treatment of the shell model can be found in almost any text-book on nuclear physics, e.g., Ref. [8, 9].

Figure 11 illustrates some of these shell model orbits and a few possibilities of how to fill them with particles in ^{39}K. Four different excitation modes for ^{39}K are shown in the figure. Also, note in the figure the number of particles and holes on respective sides of the major shells defined by the energy gap at nucleon number 20. For example, *1p-2h* means one particle in the $1f_{7/2}$ level and two holes in the $1d_{3/2}$ level, with no distinction made between neutrons and protons. In the first case (Figure 11 (A)) the experimentally known $3/2^+$ ground state can be easily understood, as there is one odd particle (hole) in the $1d_{3/2}$ level (positive parity). In terms of particles, two of the protons in that same orbital have to couple to spin $I = 0$, and the unpaired proton yields $3/2^+$. Since a particle and a hole behave analogously, the situation could also be regarded as if there is one hole in the $1d_{3/2}$ level, giving $I^\pi = 3/2^+$ as the only possibility.

The second lowest energy level arises if the pair in the $2s_{1/2}$ shell is broken, and one of the protons is excited to the $1d_{3/2}$ level, resulting in a $1/2^+$ state. Since only yrast states can be seen in the data from this experiment, this state is not observed. It is, however, known and has an energy of 2523 keV, i.e., below the first excited level (2813 keV) shown in Figure 10. If instead, the odd proton in the $1d_{3/2}$ orbit is excited to the $1f_{7/2}$ level, as shown in part B of Figure 11, and if at the same time, the two remaining protons in $1d_{3/2}$ couple to spin 0, the total spin will equal the spin for the odd proton in $1f_{7/2}$, giving $I^\pi = 7/2^-$ (negative parity because f means $\ell = 3$, odd). By looking at the level scheme in Figure 10, this state is found at 2813 keV, the first excited high-spin state. This makes sense, since we cannot see the $1/2^+$ state arising from (A) and the $7/2^-$ state is apparently the second excited state. If we break the pair left in the $1d_{3/2}$ shell, the resultant spin in this shell could take on values between $3/2 + 3/2 = 3$ and $3/2 - 3/2 = 0$, in integer steps. However, since the two protons must be treated as identical particles (fermions which obey the Pauli principle) they must be described by an anti-symmetrized total wave function. This restricts the possible spins to even values, i.e., 0^+ or 2^+. Thus, the possible total spins of the situation in part B are $I^\pi = 7/2^-$ or $11/2^-$. Again, looking at the level scheme, this $11/2^-$ state can correspond to the 3943 keV level.

If we instead of the proton excite a neutron to the $1f_{7/2}$ level, many possibilities open up to form excited states (Figure 11, part C). The excited neutron gives rise to spin $7/2^-$ and the odd neutron and the odd proton, both in the $1d_{3/2}$ level, couple their spins both parallel and anti-parallel since they are non-identical particles. Possible values from this coupling are thus $I = 0^+, 1^+, 2^+, 3^+$, where the even angular momenta correspond to the two particles having their spins anti-parallel. The total spin can then be $7/2^-, 9/2^-, 11/2^-$ or $13/2^-$ for the excitation mode in part C. Except for the $7/2^-$ state, possible candidates for all these total spins can be found in the level scheme. Since there are more than one level with for example $11/2^-$ relatively close to each other, we cannot decide which of the levels that actually corresponds to this $11/2^-$ state, from only this simple reasoning.

In part D of Figure 11 both a proton and a neutron are excited across the $N, Z = 20$ gap to the $1f_{7/2}$ level, leaving us with two odd particles and an odd hole: a neutron and a proton in $1f_{7/2}$ and a neutron hole in $1d_{3/2}$. The two protons in $1d_{3/2}$ can couple their spins to a maximum of 2, like in case B above and the maximum value after coupling is thus $21/2^+$. The other possibility is when the two protons couple to 0, giving a total of $17/2^+$. Both these states can be found in the level scheme at 11691 keV and 7775 keV respectively.

From the simple reasoning above, based on the basic assumptions of the nuclear shell model, many of the low-lying states can be understood. The same reasoning can also be performed for ^{39}Ca, only switch neutrons with protons and vice versa.

4.2 Shell Model Calculations

Compared to the naive discussion above, theoreticians have much more elaborate ways of calculating levels in a nucleus. With different models and modifications of the shell model, they can reproduce states much higher up in excitation energy. Some shell model calculations for ^{39}K have been made [10], but the results will not be presented within the realms of this work.

4.3 Mirror Symmetry

The shell model is especially successful for explaining the properties of nuclei with one nucleon too many or too few. The two nuclei studied in this work, ^{39}K and ^{39}Ca, are so called mirror nuclei, i.e., the neutron number of the one equals the proton number of the other and vice versa. As can be seen by the comparison of the two nuclei in Figure 7 the nuclear structures are very similar. This is a consequence of the nuclear force not distinguishing between neutrons and protons. The small difference in Figure 7

can be interpreted as electromagnetic effects. The total difference in Coulomb energy between these two nuclei is about 8 MeV, but if the level schemes are placed next to each other with the ground states at the same level, like in Figure 7, plotting the difference of the (internal) Coulomb energies between the two nuclei reveals an almost straight line; only the positive parity state deviates considerably from this line. The shell model still holds ...

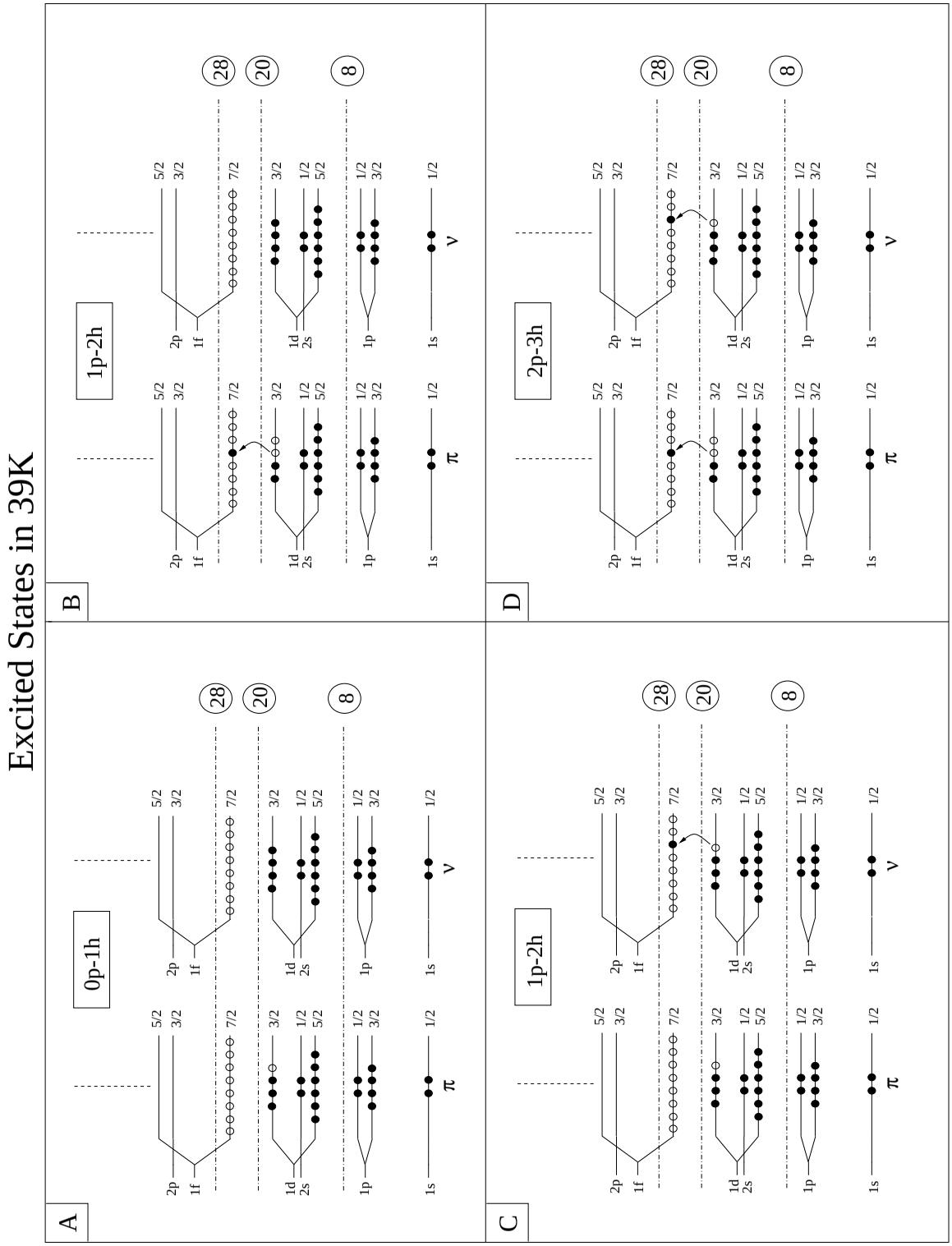

Figure 11: Four different modes of excitation in ^{39}K. The xp-yh notation describes the number of particles above and holes below the $N, Z = 20$ gap. π and ν denotes protons and neutrons, respectively.

Acknowledgements

At the time of the experiment, neither had I given my master thesis even as much as a thought, nor was I present during the run. Therefore I was more than delighted to learn that I, as a part of my project, would get the chance to accompany the Lund Nuclear Structure Group to an experiment at the EUROBALL facility in Legnaro, Italy. EUROBALL is in many aspects a very similar sort of detector system as GAMMASPHERE, making the experimental procedures rather identical. Night shifts, tuning problems, changing of targets and other blood-curdling experiences, but also enjoyable dinners and pleasant company, all have I now experienced. Thus, I have convinced myself that I now know how an experiment is performed. It kind of makes you appreciate the data a little more.

For the very professional and friendly guidance, advice and help during the progress of this work, I especially wish to thank Dr. Dirk Rudolph and Prof. Claes Fahlander and the other members of the Nuclear Structure Group. A little token of gratitude also goes to my dear computer for only breaking down once.

References

[1] GAMMASPHERE Users Executive Committee, GAMMASPHERE*: The Beginning...1993-1997* (see also http://www-gam.lbl.gov)

[2] D. G. Sarantites *et al.*, Nucl. Instr. Meth. Phys. Res. **A381** 418 (1996)

[3] D. C. Radford, *ESCL8R and LEVIT8R: Software for Interactive Graphical Analysis of HPGe Coincidence Data Sets*, Nucl. Instr. Meth. Phys. Res. **A361** 297 (1995)

[4] M. K. Kabadiyski *et al.*, Nucl. Phys. **A563** 301 (1993)

[5] K.S. Krane, R.M. Steffen, R.M. Wheeler, At. Data Nucl. Data Tables **11** 351 (1973)

[6] P.M. Endt, Nucl. Phys. **A521** 1 (1990)

[7] H. H. Eggenhuisen *et al.*, Nucl. Phys. **A305** 245 (1978)

[8] K. S. Krane, *Introductory Nuclear Physics*, Wiley & Sons, 1988

[9] B. Povh, K. Rith, C. Scholz, F. Zetsche, *Particles and Nuclei: An Introduction to the Physical Concepts*, Springer Verlag, 1995

[10] B. A. Brown, Private Communications

A Tables

Table 1: The different rings and pseudo-rings (see Section 3.3) for the Ge detectors in the GAMMASPHERE array.

Ring No.	Detector angle	No. of detectors	Pseudo-ring No.	No. of detectors & 'Angle' in pseudo-ring
1	17.3°	0		
2	31.7°	0		
3	37.4°	0		
4	50.1°	10	1	30 ⇒ '53'
5	58.3°	5	1	
6	69.8°	8	2	15 ⇒ '70'
7	79.2°	4	3	23 ⇒ '83'
8	80.7°	3	3	
9	90.0°	7	3	
10	99.3°	5	3	
11	100.8°	4	3	
12	110.2°	7	2	
13	121.7°	5	1	
14	129.9°	10	1	
15	142.6°	5	4	15 ⇒ '30'
16	148.3°	5	4	
17	162.7°	5	4	
	Total: 83			Total: 83

Table 2: Coincidence matrix for γ-ray transitions in ^{39}Ca. 'X' notates strong coincidence, 'x' less strong coincidence, and '-' no coincidence. Contaminations are marked with 'c', and for unclear cases a question mark '?' is used. All energies given in keV.

	Coincident Transition											
Gate	252	842	849	1030	1094	1259	1510	1748	1872	2795	3006	3637
252	-	X	X	X	-	X	X	X	x	X	X	X
842	X	-	x	?	-	x	-	?	-	X	X	-
849	X	X	-	?	X	x	-	X	?	X	X	-
1030	x	x	-	-	x	-	X	-	-	X	-	-
1094	-	-	X	x	-	x	x	x	-	X	X	-
1259	X	x	x	-	X	-	c	x	?	X	c	-
1510	x	-	-	X	x	c	-	-	-	X	-	-
1748	x	X	X	-	X	X	-	-	-	X	-	-
1872	-	-	-	-	-	-	-	-	-	-	-	-
2795	X	X	X	x	X	X	X	x	x	-	X	-
3006	X	X	X	-	x	c	-	-	-	x	-	-

Table 3: Energies for the excited states in ^{39}Ca, transition energies, and relative intensities.

E_x (keV)	E_γ (keV)	I_{rel} (%)
2795.0(15)	2795(2)	100(10)
3637.0(15)	3637(2)	12(3)
	842(1)	34(5)
3889.0(16)	252(1)	38(4)
	1094(1)	74(9)
5147.8(18)	1259(1)	27(2)
5399.0(19)	1510(1)	28(2)
6429.0(21)	1030(1)	20(2)
6895.7(20)	3006(2)	33(3)
	1748(1)	24(2)
7744.7(22)	849(1)	45(6)

Table 4: Energies for the excited states in ^{39}K, transition energies, relative intensities, DCO ratios calculated from three different gates, and tentative spins and parities of the initial and final states.

E_x (keV)	E_γ (keV)	I_{rel} (%)	R_{DCO} (30° − 83°) 2813 keV	1130 keV	887 keV	Multipole assignment	I_i^π ($\hbar$)	I_f^π ($\hbar$)
2813.4(10)	2813.0(7)	100(3)	-	1.02(5)	0.98(5)	$M2$	$7/2^-$	$3/2^+$
3596.3(10)	3597.0(9)	28(1)	-	-	?	$E3$	$9/2^-$	$3/2^+$
	782.7(2)	51(2)	1.14(6)	-	1.18(7)	$E2/M1$	$9/2^-$	$7/2^-$
3943.0(10)	346.7(1)	50(2)	0.66(3)	-	0.62(3)	$E2/M1$	$11/2^-$	$9/2^-$
	1129.9(3)	72(2)	1.04(5)	-	1.09(5)	$E2$	$11/2^-$	$7/2^-$
4518.5(17)	922		?	-	-	$\Delta I = 0$	$9/2^-$	$9/2^-$
5352.2(11)	1409.5(4)	28(1)	1.25(8)	0.93(6)	0.91(5)	$\Delta I = 0$	$11/2^-$	$11/2^-$
	834		-	-	-	$E2/M1$	$11/2^-$	$9/2^-$
5716.2(11)	1773.2(4)	59(2)	0.86(5)	0.88(5)	-	$E2/M1$	$13/2^-$	$11/2^-$
	364.1(1)	1.1(1)	0.94(22)	0.45(11)	-	$E2/M1$	$13/2^-$	$11/2^-$
6005.1(13)	2062.1(5)	5.4(2)	1.19(19)	1.29(18)	-	$\Delta I = 0$	$11/2^-$	$11/2^-$
6433.5(12)	2490.0(6)	28(1)	0.66(5)	0.62(4)	-	$E1$	$13/2^+$	$11/2^-$
6473.3(12)	756.8(2)	42(1)	0.62(3)	0.73(3)	-	$E1$	$15/2^+$	$13/2^-$
7140.4(12)	3196.7(8)	35(1)	1.17(7)	1.15(7)	1.10(6)	$E2$	$15/2^-$	$11/2^-$
	1134.6		-	-	-	$E2$	$15/2^-$	$11/2^-$
	1788.2(4)	27(1)	1.26(11)	1.19(11)	1.13(6)	$E2$	$15/2^-$	$11/2^-$
	1426.6(4)	4.2(1)	0.98(17)	-	-	$E2/M1$	$15/2^-$	$13/2^-$
7567.3(12)	1094.3(3)	5.2(2)	1.28(13)	-	-	$\Delta I = 0$	$15/2^+$	$15/2^+$
	1849.8(5)	3.6(1)	0.71(13)	-	-	$E1$	$15/2^+$	$13/2^-$
7775.4(12)	1341.8(3)	24(1)	1.13(7)	1.06(6)	-	$E2$	$17/2^+$	$13/2^+$
	635.8(2)	0.8(1)	0.70(38)	-	-	$E1$	$17/2^+$	$15/2^-$
	1301.2(3)	20(1)	0.27(2)	0.35(5)	-	$E2/M1$	$17/2^+$	$15/2^+$
8008.5(14)	4066.1(10)	2.5(1)	-	1.27(40)	-	$E2/M1$	$(13/2^-)$	$11/2^-$
	2655.0		-	-	-	$E2/M1$	$(13/2^-)$	$11/2^-$
	2044.0		-	-	-	$E2/M1$	$(13/2^-)$	$11/2^-$
8018.3(22)	1545		-	-	-	-	-	$15/2^+$
8027.4(12)	886.6(2)	45(1)	1.20(6)	1.07(5)	-	$E2$	$19/2^-$	$15/2^-$
	252.1(1)	5.8(2)	0.63(5)	0.79(7)	-	$E1$	$19/2^-$	$17/2^+$
8681.1(13)	2207.6(6)	5.2(2)	-	-	-	$\Delta I = 0$	$(15/2^+)$	$15/2^+$
	1113.0		-	-	-	$\Delta I = 0$	$(15/2^+)$	$15/2^+$
9270.7(14)	2130.4(5)	11(1)	1.40(17)	1.05(10)	-	$E2$	$(19/2^-)$	$15/2^-$
9363.4(13)	2891.2(7)	6.0(2)	0.95(12)	1.79(31)	-	$E2/M1$	$(17/2^+)$	$15/2^+$
	682.3(2)	1.5(1)	0.78(10)			$E2/M1$	$(17/2^+)$	$(15/2^+)$

Continued on next page.

Table 4: Continued...

E_x (keV)	E_γ (keV)	I_{rel} (%)	R_{DCO} (30° − 83°) 2813 keV	1130 keV	887 keV	Multipole assignment	I_i^π ($\hbar$)	I_f^π ($\hbar$)
9907.6(14)	1880.6(5)	16(1)	1.23(11)	1.23(9)	1.11(6)	$E2/M1$	$(21/2^-)$	$19/2^-$
10264.0(15)	2255.5(6)	6.2(2)	0.93(18)	-	-	$E2$	$(17/2^-)$	$(13/2^-)$
	3123.5(8)	4.2(1)	0.96(14)	0.97(13)	-	$E2/M1$	$(17/2^-)$	$15/2^-$
10278.0(15)	2503		-	-	-	$E2/M1$	$(19/2^+)$	$17/2^+$
	2710		-	-	-	$E2$	$(19/2^+)$	$15/2^+$
	914		1.09(22)	-	-	$E2/M1$	$(19/2^+)$	$(17/2^+)$
10303.2(13)	2527.2(6)	15(1)	1.54(12)	1.54(14)	-	$E2/M1$	$19/2^+$	$17/2^+$
	939.8(2)	1.5(1)	0.69(16)	-	-	$E2/M1$	$19/2^+$	$(17/2^+)$
10383.0(14)	3908		1.18(33)	-	-	$E2$	$(19/2^+)$	$15/2^+$
	2607.8(7)	6.0(2)	0.90(12)	1.39(22)	-	$E2/M1$	$(19/2^+)$	$17/2^+$
10882.4(17)	3315.1(8)	1.8(1)	-	-	-	-	-	$17/2^+$
	4409.2(11)	1.2(1)	-	-	-	-	-	$15/2^+$
10997.0(14)	2969.9(7)	16(1)	1.09(8)	1.20(10)	1.29(8)	$E2$	$(23/2^-)$	$19/2^-$
	1727		-	-	-	$E2$	$(23/2^-)$	$(19/2^-)$
11590.1(22)	2909		1.37(32)	-	-	$E2$	$(19/2^+)$	$(15/2^+)$
11690.8(13)	3914.8(10)	2.3(1)	-	1.82(60)	-	$E2$	$(21/2^+)$	$17/2^+$
12069.1(13)	1766		-	-	-	$E2$	$(23/2^+)$	$19/2^+$
	378.3(1)	1.1(1)	0.37(16)	0.36(8)	-	$E2/M1$	$(23/2^+)$	$(21/2^+)$
	1685.9(4)	8.1(2)	1.16(12)	1.04(14)	-	$E2$	$(23/2^+)$	$(19/2^+)$
	1790		-	-	-	$E2$	$(23/2^+)$	$(19/2^+)$
12209.0(13)	2301.8(6)	4.3(1)	-	-	0.66(8)	$E2/M1$	$(23/2^-)$	$(21/2^-)$
	1212.3(3)	1.6(1)	-	-	-	$E2/M1$	$(23/2^-)$	$(23/2^-)$
	4181.2(10)	3.2(1)	-	-	-	$E2$	$(23/2^-)$	$19/2^-$
12355.2(20)	3084.5(8)	4.9(2)	0.84(15)	1.46(28)	-	-	-	$(19/2^-)$
12615.5(26)	4607.0(12)	0.2(1)	-	-	-	-	-	$(13/2^-)$
12893.0(19)	2010.6(5)	4.6(2)	-	-	-	-	-	-
13009.5(20)	2745.5(7)	5.0(2)	1.65(26)	1.10(15)	-	-	-	$(17/2^-)$
13265.7(13)	1196.3(3)	8.4(3)	0.55(5)	0.78(5)	-	$E2/M1$	$(25/2^+)$	$(23/2^+)$
	1057.1(3)	3.5(1)	0.80(13)	-	0.58(7)	$E1$	$(25/2^+)$	$(23/2^-)$
	2266		-	-	-	$E1$	$(25/2^+)$	$(23/2^-)$
13506.3(21)	3599		1.70(37)	1.44(22)	-	$E2/M1$	$(23/2^-)$	$(21/2^-)$
13776.4(24)	2186.3(5)	5.9(2)	-	-	-	-	-	$(19/2^+)$
14060.6(14)	1991.7(5)	8.7(3)	1.11(16)	?	-	$E2$	$(27/2^+)$	$(23/2^+)$
	794.9(2)	7.3(2)	0.80(7)	0.78(7)	0.99(14)	$E2/M1$	$(27/2^+)$	$(25/2^+)$
14865.3(21)	3868.0(10)	5.0(2)	-	1.23(20)	-	-	-	$(23/2^-)$
16139.5(27)	3130		-	-	-	-	-	-
18530.9(24)	4470.3(11)	2.9(1)	-	-	-	-	-	$(27/2^+)$
18611.0(23)	5105.2(13)	0.7(1)	-	-	-	-	-	$(23/2^-)$
	3745.5(9)	2.2(1)	-	-	-	-	-	-